Electronic Supplementary Material (ESI) for Physical Chemistry Chemical Physics

Supporting information for: Characterization and optimization of tartrate-based TACE inhibitors through Hamiltonian Replica Exchange

Carlo Guardiani and Piero Procacci*

Department of Chemistry, University of Florence, Italy

E-mail: piero.procacci@unifi.it

*To whom correspondence should be addressed

Force field parameters

Figure 1: Atom names of Drug-1 and Drug-6.

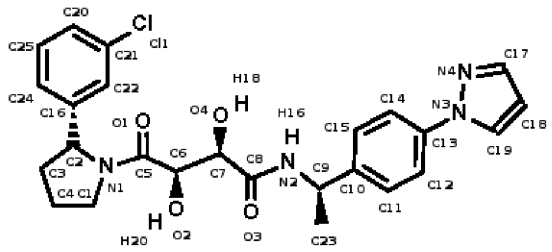

Drug-1

Drug-6RS

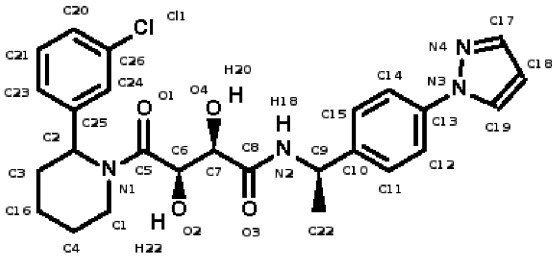

Figure 2: Atom names of Drug-38 and Drug-39.

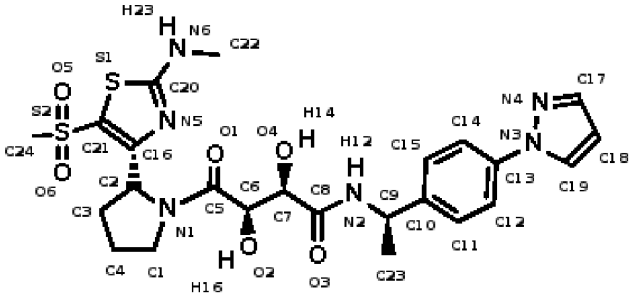

Drug-38

Drug-39RS

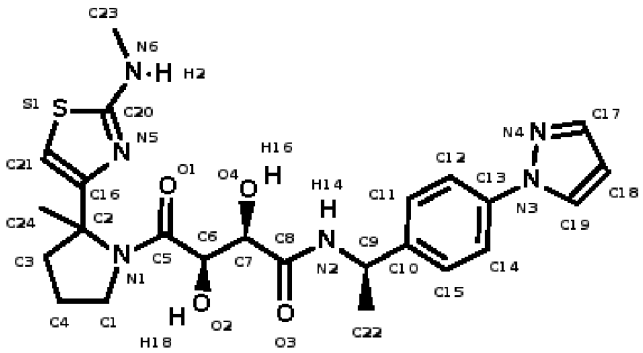

Figure 3: Atom names of Drug-43 and Drug-44.

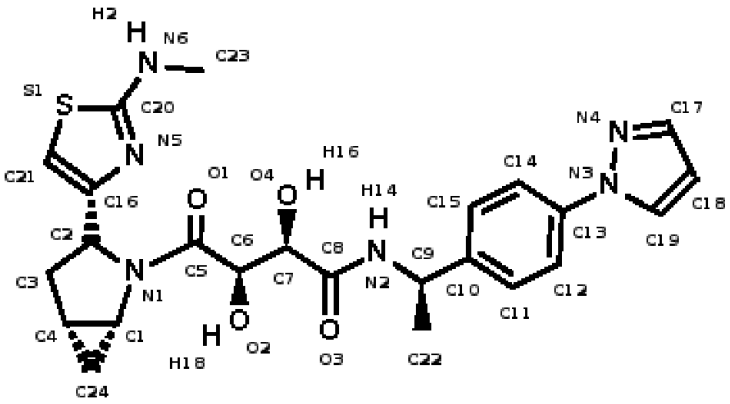

Drug-43

Drug-44

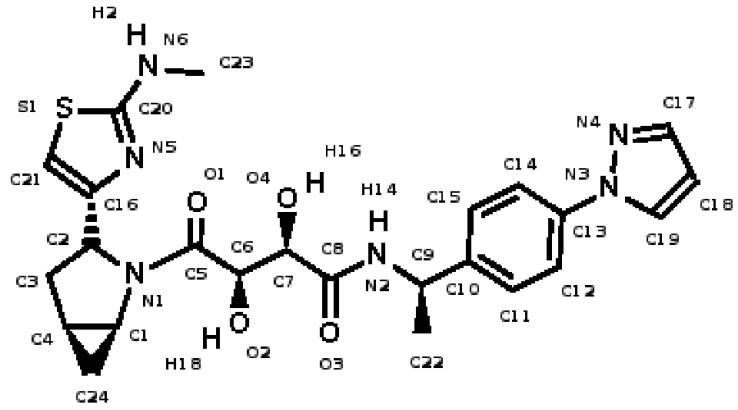

Figure 4: Atom names of drug IK682.

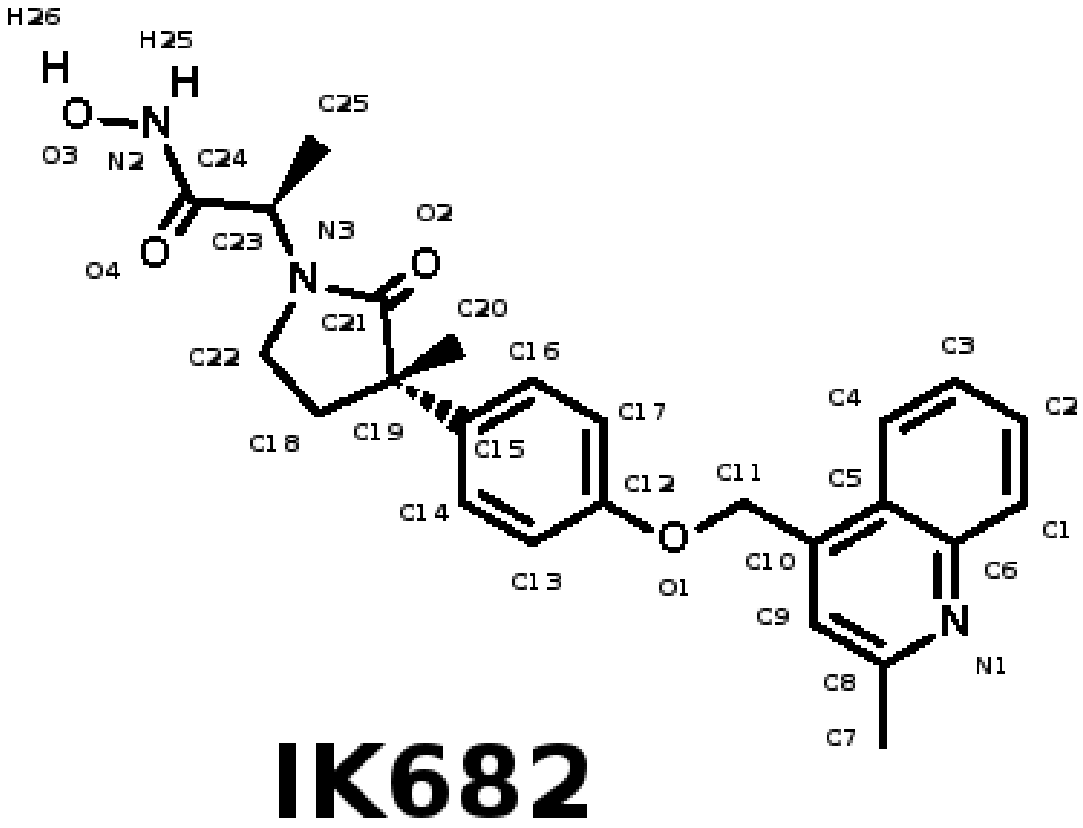

Figure 5: Atom names of compound Quino-1.

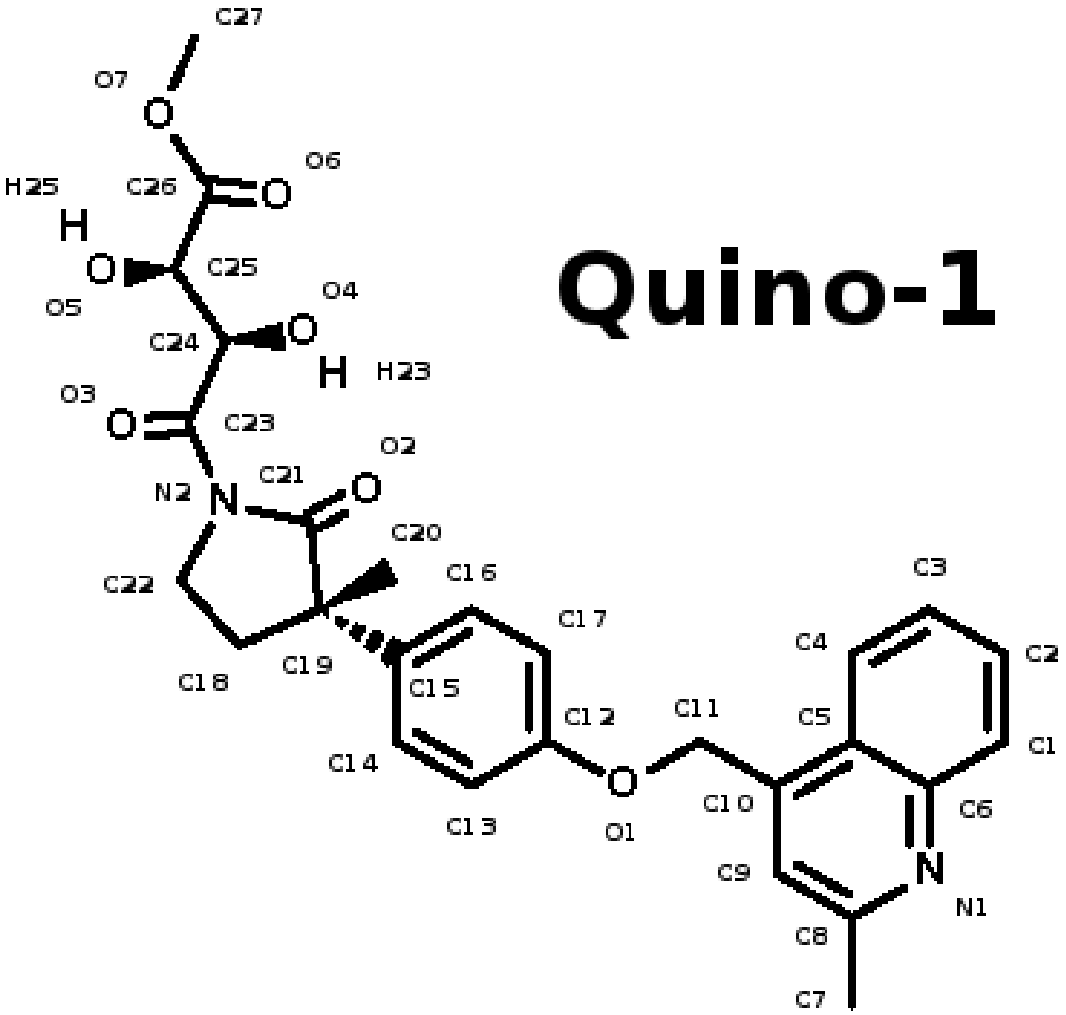

Figure 6: Atom names of compound Quino-2.

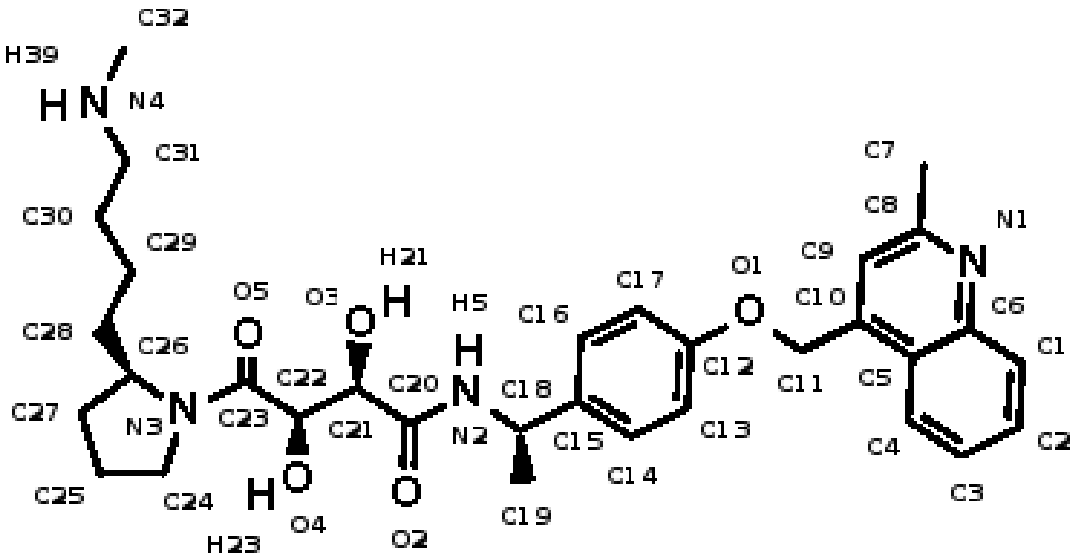

Quino-2

Table 1: Atomic charges (in electrons) of drug-1. The atom types are those defined in the GAFF force field.

Atom	Atom Type	Charge	Atom	Atom Type	Charge
C1	c3	-0.016391	H21	h1	0.039305
H22	h1	0.039305	N1	n	-0.101946
C2	c3	-0.004756	H27	h1	0.112603
C3	c3	-0.180921	H25	hc	0.078957
H26	hc	0.078957	C4	c3	0.030610
H23	hc	0.020823	H24	hc	0.020823
C16	ca	0.061114	C24	ca	-0.090690
H3	ha	0.124085	C22	ca	-0.085961
H2	ha	0.122635	C21	ca	-0.036061
Cl1	cl	-0.117335	C20	ca	-0.022692
H1	ha	0.126094	C25	ca	-0.251779
H4	ha	0.169458	C5	c	0.349103
O1	o	-0.575329	C6	c3	0.428060
H19	h1	0.001602	O2	oh	-0.753523
H20	ho	0.464712	C7	c3	0.115620
H17	h1	0.072189	O4	oh	-0.695253
H18	ho	0.442875	C8	c	0.758463
O3	o	-0.656864	N2	n	-0.703050
H16	hn	0.375329	C9	c3	0.262970
H12	h1	0.109846	C23	c3	-0.504296
H13	hc	0.140118	H14	hc	0.140118
H15	hc	0.140118	C10	ca	0.036603
C15	ca	-0.160739	H9	ha	0.144273
C14	ca	-0.163711	H8	ha	0.142409
C13	ca	0.013042	C11	ca	-0.160739
H11	ha	0.144273	C12	ca	-0.163711
H10	ha	0.142409	N3	na	0.369273
N4	nc	-0.441974	C17	cd	0.060299
H5	h4	0.144535	C18	cd	-0.291370
H6	ha	0.184432	C19	cc	-0.211842
H7	h4	0.183490			

Table 2: Atomic charges (in electrons) of drug-6R and drug-6S. The atom types are those defined in the GAFF force field.

Atom	Atom Type	Charge	Atom	Atom Type	Charge
C1	c3	0.057326	H23	h1	0.027712
H24	h1	0.027712	N1	n	-0.407385
C2	c3	0.038103	H1	h1	0.091805
C4	c3	0.064446	H25	hc	-0.013245
H26	hc	-0.013245	C16	c3	0.050044
H2	hc	-0.010988	H3	hc	-0.010988
C3	c3	0.013211	H27	hc	0.015163
H28	hc	0.015163	C25	ca	-0.011665
C23	ca	-0.087167	H6	ha	0.123857
C24	ca	-0.075117	H29	ha	0.119147
C26	ca	-0.011451	Cl1	cl	-0.126292
C20	ca	-0.047358	H4	ha	0.128121
C21	ca	-0.215072	H5	ha	0.160413
C5	c	0.682415	O1	o	-0.557210
C6	c3	0.069623	H21	h1	0.102840
O2	oh	-0.676640	H22	ho	0.423306
C7	c3	0.286334	H19	h1	0.021764
O4	oh	-0.707693	H20	ho	0.442177
C8	c	0.714550	O3	o	-0.638314
N2	n	-0.688472	H18	hn	0.366957
C9	c3	0.279440	H14	h1	0.098657
C22	c3	-0.484882	H15	hc	0.134906
H16	hc	0.134906	H17	hc	0.134906
C10	ca	0.005300	C15	ca	-0.142302
H11	ha	0.139233	C14	ca	-0.168891
H10	ha	0.142889	C13	ca	0.015935
C11	ca	-0.142302	H13	ha	0.139233
C12	ca	-0.168891	H12	ha	0.142889
N3	na	0.367685	N4	nc	-0.445845
C17	cd	0.067164	H7	h4	0.142339
C18	cd	-0.298232	H8	ha	0.185327
C19	cc	-0.206618	H9	h4	0.183268

Table 3: Atomic charges (in electrons) of drug-39R and drug-39S. The atom types are those defined in the GAFF force field.

Atom	Atom Type	Charge	Atom	Atom Type	Charge
C1	c3	0.168341	H19	h1	-0.017899
H20	h1	-0.017899	N1	n	-0.343065
C2	c3	0.273256	C4	c3	0.150273
H21	hc	-0.023352	H22	hc	-0.023352
C3	c3	-0.213181	H23	hc	0.074167
H24	hc	0.074167	C24	c3	-0.479009
H25	hc	0.132340	H26	hc	0.132340
H27	hc	0.132340	C16	cc	0.200442
N5	nc	-0.526042	C21	cd	-0.388867
H1	h4	0.272956	C20	cd	0.562358
S1	ss	-0.065141	N6	nh	-0.649244
H2	hn	0.384654	C23	c3	-0.016450
H28	h1	0.075516	H29	h1	0.075516
H30	h1	0.075516	C5	c	0.595253
O1	o	-0.616878	C6	c3	0.154127
H17	h1	0.099347	O2	oh	-0.664282
H18	ho	0.423955	C7	c3	0.162199
H15	h1	0.015738	O4	oh	-0.749490
H16	ho	0.481526	C8	c	0.820984
O3	o	-0.671999	N2	n	-0.736931
H14	hn	0.404029	C9	c3	0.295269
H10	h1	0.097400	C22	c3	-0.470725
H11	hc	0.128475	H12	hc	0.128475
H13	hc	0.128475	C10	ca	0.032115
C11	ca	-0.153155	H8	ha	0.138723
C12	ca	-0.163068	H6	ha	0.141582
C13	ca	-0.005661	C15	ca	-0.153155
H9	ha	0.138723	C14	ca	-0.163068
H7	ha	0.141582	N3	na	0.386414
N4	nc	-0.448841	C17	cd	0.066452
H3	h4	0.142008	C18	cd	-0.302868
H4	ha	0.185580	C19	cc	-0.210394
H5	h4	0.181404			

Table 4: Atomic charges (in electrons) of drug-38. The atom types are those defined in the GAFF force field.

Atom	Atom Type	Charge	Atom	Atom Type	Charge
C1	c3	-0.027882	H17	h1	0.044968
H18	h1	0.044968	N1	n	-0.215902
C2	c3	0.117580	H30	h1	0.110952
C4	c3	0.166984	H19	hc	-0.011807
H20	hc	-0.011807	C3	c3	-0.367520
H21	hc	0.121334	H22	hc	0.121334
C16	cc	0.122191	C21	cd	-0.185498
N5	nc	-0.217403	C20	cd	0.345479
S1	ss	-0.082553	S2	sy	1.038850
O5	o	-0.545877	O6	o	-0.545877
C24	c3	-0.460459	H27	h1	0.162262
H28	h1	0.162262	H29	h1	0.162262
N6	nh	-0.600650	H23	hn	0.425257
C22	c3	-0.041322	H24	h1	0.084164
H25	h1	0.084164	H26	h1	0.084164
C5	c	0.481712	O1	o	-0.577868
C6	c3	0.298368	H15	h1	0.033877
O2	oh	-0.726452	H16	ho	0.453364
C7	c3	0.097746	H13	h1	0.020068
O4	oh	-0.693029	H14	ho	0.449160
C8	c	0.846953	O3	o	-0.675535
N2	n	-0.720504	H12	hn	0.365378
C9	c3	0.387850	H8	h1	0.074247
C23	c3	-0.541873	H9	hc	0.141942
H10	hc	0.141942	H11	hc	0.141942
C10	ca	-0.057301	C11	ca	-0.134721
H6	ha	0.145441	C12	ca	-0.176728
H4	ha	0.143058	C13	ca	0.021793
C15	ca	-0.134721	H7	ha	0.145441
C14	ca	-0.176728	H5	ha	0.143058
N3	na	0.372345	N4	nc	-0.447081
C17	cd	0.064671	H1	h4	0.142999
C18	cd	-0.295091	H2	ha	0.185396
C19	cc	-0.208913	H3	h4	0.183178

Table 5: Atomic charges (in electrons) of drug-43 and drug-44. The atom types are those defined in the GAFF force field.

Atom	Atom Type	Charge	Atom	Atom Type	Charge
C1	cx	-0.088766	H20	h1	0.094740
N1	n	-0.022194	C2	c3	0.208728
H23	h1	0.057032	C4	cx	0.069424
H19	hc	0.105149	C24	cx	-0.370242
H24	hc	0.144044	H25	hc	0.144044
C3	c3	-0.499109	H21	hc	0.182338
H22	hc	0.182338	C16	cc	0.135717
C21	cd	-0.321216	H1	h4	0.244874
N5	nc	-0.716617	C20	cd	0.743772
S1	ss	-0.093009	N6	nh	-0.715209
H2	hn	0.401324	C23	c3	0.104165
H26	h1	0.039255	H27	h1	0.039255
H28	h1	0.039255	C5	c	0.457258
O1	o	-0.634520	C6	c3	0.319399
H17	h1	0.021896	O2	oh	-0.745170
H18	ho	0.467553	C7	c3	0.219612
H15	h1	0.057778	O4	oh	-0.703286
H16	ho	0.431766	C8	c	0.680520
O3	o	-0.636782	N2	n	-0.639810
H14	hn	0.349200	C9	c3	0.355198
H10	h1	0.086733	C22	c3	-0.551923
H11	hc	0.143277	H12	hc	0.143277
H13	hc	0.143277	C10	ca	-0.034079
C11	ca	-0.150295	H8	ha	0.148741
C12	ca	-0.167035	H6	ha	0.140423
C13	ca	0.026894	C15	ca	-0.150295
H9	ha	0.148741	C14	ca	-0.167035
H7	ha	0.140423	N3	na	0.357747
N4	nc	-0.441270	C17	cd	0.063897
H3	h4	0.141877	C18	cd	-0.295692
H4	ha	0.183443	C19	cc	-0.200513
H5	h4	0.179685			

Table 6: Atomic charges (in electrons) of drug IK682. The atom types are those defined in the GAFF force field.

Atom	Atom Type	Charge	Atom	Atom Type	Charge
C1	ca	-0.311301	H2	ha	0.175766
C2	ca	-0.105982	H1	ha	0.146204
C3	ca	-0.183221	H3	ha	0.151851
C4	ca	-0.137189	H4	ha	0.126672
C5	ca	-0.245370	C6	ca	0.605589
N1	nb	-0.766828	C8	ca	0.712199
C7	c3	-0.361161	H6	hc	0.097469
H7	hc	0.097469	H8	hc	0.097469
C9	ca	-0.597878	H5	ha	0.232392
C10	ca	0.226387	C11	c3	0.164829
H9	h1	0.059418	H10	h1	0.059418
O1	os	-0.417676	C12	ca	0.403024
C13	ca	-0.286413	H11	ha	0.166000
C14	ca	-0.186616	H14	ha	0.170302
C17	ca	-0.286413	H12	ha	0.166000
C16	ca	-0.186616	H13	ha	0.170302
C15	ca	0.055450	C19	c3	0.082342
C20	c3	-0.338037	H15	hc	0.101381
H16	hc	0.101381	H17	hc	0.101381
C18	c3	-0.351562	H18	hc	0.115247
H19	hc	0.115247	C22	c3	0.124867
H20	h1	0.039258	H21	h1	0.039258
C21	c	0.687966	O2	o	-0.651734
N3	n	-0.315899	C23	c3	0.059967
H27	h1	0.051642	C25	c3	-0.276691
H22	hc	0.093813	H23	hc	0.093813
H24	hc	0.093813	C24	c	0.688372
O4	o	-0.571167	N2	n	-0.516413
H25	hn	0.430150	O3	oh	-0.431492
H26	ho	0.421553			

Table 7: Atomic charges (in electrons) of drug Quino-1. The atom types are those defined in the GAFF force field.

Atom	Atom Type	Charge	Atom	Atom Type	Charge
C1	ca	-0.322184	H3	ha	0.177899
C2	ca	-0.100184	H2	ha	0.146292
C3	ca	-0.184692	H4	ha	0.152309
C4	ca	-0.136139	H5	ha	0.127595
C5	ca	-0.250593	C10	ca	0.210016
C6	ca	0.623975	N1	nb	-0.769463
C8	ca	0.710916	C9	ca	-0.592983
H6	ha	0.230431	C7	c3	-0.363211
H7	hc	0.098760	H8	hc	0.098760
H9	hc	0.098760	C11	c3	0.178497
H10	h1	0.057339	H11	h1	0.057339
O1	os	-0.419581	C12	ca	0.373417
C13	ca	-0.254972	H12	ha	0.166195
C14	ca	-0.186136	H15	ha	0.168183
C16	ca	-0.186136	H14	ha	0.168183
C17	ca	-0.254972	H13	ha	0.166195
C15	ca	-0.010699	C19	c3	0.285205
C18	c3	-0.589363	H19	hc	0.171312
H20	hc	0.171312	C22	c3	0.317754
H21	h1	0.009704	H22	h1	0.009704
N2	n	-0.246856	C21	c	0.429269
O2	o	-0.540907	C20	c3	-0.371144
H16	hc	0.110436	H17	hc	0.110436
H18	hc	0.110436	C23	c	0.386395
O3	o	-0.513128	C24	c3	0.613878
H1	h1	-0.038204	O4	oh	-0.712337
H23	ho	0.444253	C25	c3	-0.051655
H24	h1	0.097781	O5	oh	-0.673997
H25	ho	0.466213	C26	c	0.770583
O6	o	-0.601426	O7	os	-0.363100
C27	c3	-0.122669	H26	h1	0.113666
H27	h1	0.113666	H28	h1	0.113666

Table 8: Charges (in electrons) and atom-types (GAFF) of Quino-2.

Atom	Atom Type	Charge	Atom	Atom Type	Charge
C1	ca	-0.314772	H7	ha	0.175992
C2	ca	-0.104361	H6	ha	0.145571
C3	ca	-0.184889	H8	ha	0.152158
C4	ca	-0.146168	H9	ha	0.131817
C5	ca	-0.222824	C10	ca	0.190336
C6	ca	0.602963	N1	nb	-0.768231
C7	c3	-0.383653	H11	hc	0.102380
H12	hc	0.102380	H13	hc	0.102380
C8	ca	0.719016	C9	ca	-0.590764
H10	ha	0.225857	C11	c3	0.191762
H14	h1	0.052001	H15	h1	0.052001
O1	os	-0.416377	C12	ca	0.394654
C13	ca	-0.289377	H16	ha	0.172593
C14	ca	-0.142651	H19	ha	0.148920
C16	ca	-0.142651	H18	ha	0.148920
C17	ca	-0.289377	H17	ha	0.172593
C15	ca	-0.075697	C18	c3	0.404618
H1	h1	0.067537	N2	n	-0.640652
H5	hn	0.351637	C19	c3	-0.526133
H2	hc	0.133107	H3	hc	0.133107
H4	hc	0.133107	C20	c	0.621408
O2	o	-0.605359	C21	c3	0.132165
H20	h1	0.046983	O3	oh	-0.723701
H21	ho	0.457775	C22	c3	0.328704
H22	h1	0.038719	O4	oh	-0.712364
H23	ho	0.459323	C23	c	0.417745
O5	o	-0.541944	N3	n	-0.172094
C26	c3	0.098367	H30	h1	0.072372
C24	c3	-0.013866	H24	h1	0.059800
H27	h1	0.059800	C25	c3	-0.017342
H25	hc	0.032782	H26	hc	0.032782
C27	c3	-0.212063	H28	hc	0.069468
H29	hc	0.069468	C28	c3	0.032963
H31	hc	0.003168	H32	hc	0.003168
C29	c3	0.046692	H33	hc	-0.028723
H34	hc	-0.028723	C30	c3	0.013885
H35	hc	-0.005418	H36	hc	-0.005418
C31	c3	0.198716	H37	h1	0.012710
H38	h1	0.012710	N4	n3	-0.761889
H39	hn	0.365046	C32	c3	0.072670
H40	h1	0.033562	H41	h1	0.033562
H42	h1	0.033562			

Clustering Analysis

Clustering analysis have been done using the Quality Threshold algorithm described in the section "Methods" of the main paper. In the following we report the results of such analysis obtained from the configurations sampled in the target replica from a 8 ns H-REM simulation at P=1 atm and T=300 K for all drugs reported in Figure 1-Figure 6.

Table 9: Clustering analysis of drug-1 in pure water (distance cutoff: 2.0 Å). The Table lists the 10 most populated clusters accounting together for 76% of the equilibrium ensemble. For each cluster the relative population and a short description of the typical structural motif are reported (COMP: compact structure; EXT: extended conformation). The population of each cluster is normalized with respect to the total equilibrium ensemble (16016 structures).

Clust	Rel. Pop.	Short Desc
1	0.24	COMP
2	0.14	COMP
3	0.07	EXT
4	0.07	COMP
5	0.07	COMP
6	0.05	COMP
7	0.05	COMP
8	0.03	COMP
9	0.02	COMP
10	0.02	EXT

Table 10: Clustering analysis of drug-6R in pure water (distance cutoff: 2.0 Å). The Table lists the 10 most populated clusters accounting together for 42% of the equilibrium ensemble. For each cluster the relative population and a short description of the typical structural motif are reported (COMP: compact structure; EXT: extended conformation). The population of each cluster is normalized with respect to the total equilibrium ensemble (16016 structures).

Clust	Rel. Pop.	Short Desc
1	0.09	EXT
2	0.05	COMP
3	0.05	EXT
4	0.05	COMP
5	0.05	COMP
6	0.03	COMP
7	0.03	COMP
8	0.03	COMP
9	0.02	COMP
10	0.02	EXT

Table 11: Clustering analysis of drug-6S in pure water (distance cutoff: 2.0 Å). The Table lists the 10 most populated clusters accounting together for 40% of the equilibrium ensemble. For each cluster the relative population and a short description of the typical structural motif are reported (COMP: compact structure; EXT: extended conformation). The population of each cluster is normalized with respect to the total equilibrium ensemble (16016 structures).

Clust	Rel. Pop.	Short Desc
1	0.07	EXT
2	0.06	EXT
3	0.04	EXT
4	0.04	COMP
5	0.04	EXT
6	0.04	COMP
7	0.03	EXT
8	0.03	COMP
9	0.03	COMP
10	0.02	EXT

Table 12: Clustering analysis of drug-39S in pure water (distance cutoff: 2.0 Å). The Table lists the 10 most populated clusters accounting together for 59% of the equilibrium ensemble. For each cluster the relative population and a short description of the typical structural motif are reported (COMP: compact structure; MED: medium compactness structure; EXT: extended conformation). The population of each cluster is normalized with respect to the total equilibrium ensemble (16016 structures).

Clust	Rel. Pop.	Short Desc
1	0.12	MED
2	0.09	MED
3	0.09	MED
4	0.08	MED
5	0.05	COMP
6	0.04	EXT
7	0.03	EXT
8	0.03	EXT
9	0.03	COMP
10	0.02	EXT

Table 13: Clustering analysis of drug-39R in pure water (distance cutoff: 2.0 Å). The Table lists the 10 most populated clusters accounting together for 40% of the equilibrium ensemble. For each cluster the relative population and a short description of the typical structural motif are reported (COMP: compact structure; EXT: extended conformation). The population of each cluster is normalized with respect to the total equilibrium ensemble (16016 structures).

Clust	Rel. Pop.	Short Desc
1	0.07	EXT
2	0.06	EXT
3	0.04	EXT
4	0.04	COMP
5	0.04	EXT
6	0.04	COMP
7	0.03	EXT
8	0.03	COMP
9	0.03	COMP
10	0.02	EXT

Table 14: Clustering analysis of drug-38 in pure water (distance cutoff: 2.0 Å). The Table lists the 10 most populated clusters accounting together for 53% of the equilibrium ensemble. For each cluster the relative population and a short description of the typical structural motif are reported (COMP: compact structure; EXT: extended conformation). The population of each cluster is normalized with respect to the total equilibrium ensemble (16016 structures).

Clust	Rel. Pop.	Short Desc
1	0.12	COMP
2	0.09	COMP
3	0.07	COMP
4	0.06	COMP
5	0.05	COMP
6	0.05	COMP
7	0.03	COMP
8	0.02	COMP
9	0.02	COMP
10	0.02	COMP

Table 15: Clustering analysis of drug-43 in pure water (distance cutoff: 2.0 Å). The Table lists the 10 most populated clusters accounting together for 72% of the equilibrium ensemble. For each cluster the relative population and a short description of the typical structural motif are reported (COMP: compact structure; EXT: extended conformation). The population of each cluster is normalized with respect to the total equilibrium ensemble (16016 structures).

Clust	Rel. Pop.	Short Desc
1	0.25	COMP
2	0.13	COMP
3	0.10	EXT
4	0.05	COMP
5	0.05	COMP
6	0.04	COMP
7	0.03	COMP
8	0.03	EXT
9	0.02	EXT
10	0.02	EXT

Table 16: Clustering analysis of drug-44 in pure water (distance cutoff: 2.0 Å). The Table lists the 10 most populated clusters accounting together for 62% of the equilibrium ensemble. For each cluster the relative population and a short description of the typical structural motif are reported (COMP: compact structure; EXT: extended conformation). The population of each cluster is normalized with respect to the total equilibrium ensemble (16016 structures).

Clust	Rel. Pop.	Short Desc
1	0.19	COMP
2	0.10	EXT
3	0.09	COMP
4	0.07	COMP
5	0.06	COMP
6	0.03	COMP
7	0.02	EXT
8	0.02	COMP
9	0.02	COMP
10	0.02	COMP

Table 17: Clustering analysis of drug-1 in DMSO (distance cutoff: 3.0 Å). The Table lists the 10 most populated clusters accounting together for 97.5% of the equilibrium ensemble. For each cluster the relative population and a short description of the typical structural motif are reported (COMP: compact structure; EXT: extended conformation). The population of each cluster is normalized with respect to the total equilibrium ensemble (16016 structures).

Clust	Rel. Pop.	Short Desc
1	0.61	COMP
2	0.18	COMP
3	0.08	COMP
4	0.03	COMP
5	0.02	COMP
6	0.02	COMP
7	0.01	EXT
8	0.01	EXT
9	0.01	EXT
10	0.005	EXT

Table 18: Clustering analysis of drug-38 in DMSO (distance cutoff: 3.0 Å). The Table lists the 10 most populated clusters accounting together for 81% of the equilibrium ensemble. For each cluster the relative population and a short description of the typical structural motif are reported (COMP: compact structure; MED: medium compactness structure; EXT: extended conformation). The population of each cluster is normalized with respect to the total equilibrium ensemble (16016 structures).

Clust	Rel. Pop.	Short Desc
1	0.26	COMP
2	0.19	MED
3	0.13	COMP
4	0.06	MED
5	0.04	COMP
6	0.03	COMP
7	0.03	EXT
8	0.03	COMP
9	0.02	COMP
10	0.02	EXT

Table 19: Clustering analysis of drug-43 in DMSO (distance cutoff: 3.0 Å). The Table lists the 10 most populated clusters accounting together for 97.9% of the equilibrium ensemble. For each cluster the relative population and a short description of the typical structural motif are reported (COMP: compact structure; EXT: extended conformation). The population of each cluster is normalized with respect to the total equilibrium ensemble (16016 structures).

Clust	Rel. Pop.	Short Desc
1	0.61	COMP
2	0.22	COMP
3	0.06	COMP
4	0.04	EXT
5	0.02	COMP
6	0.01	EXT
7	0.01	COMP
8	0.005	COMP
9	0.002	EXT
10	0.002	COMP

Table 20: Clustering analysis of drug-44 in DMSO (distance cutoff: 3.0 Å). The Table lists the 10 most populated clusters accounting together for 98.2% of the equilibrium ensemble. For each cluster the relative population and a short description of the typical structural motif are reported (COMP: compact structure; EXT: extended conformation). The population of each cluster is normalized with respect to the total equilibrium ensemble (16016 structures).

Clust	Rel. Pop.	Short Desc
1	0.64	COMP
2	0.23	COMP
3	0.04	EXT
4	0.03	COMP
5	0.01	EXT
6	0.01	EXT
7	0.01	COMP
8	0.005	COMP
9	0.005	EXT
10	0.002	EXT

Table 21: Clustering analysis of drug IK682 in water (distance cutoff: 3.0 Å). The Table lists the 10 most populated clusters accounting together for 85% of the equilibrium ensemble. For each cluster the relative population and a short description of the typical structural motif are reported (COMP: compact structure; EXT: extended conformation). The population of each cluster is normalized with respect to the total equilibrium ensemble (16016 structures).

Clust	Rel. Pop.	Short Desc
1	0.48	EXT
2	0.13	EXT
3	0.07	EXT
4	0.04	EXT
5	0.03	COMP
6	0.03	COMP
7	0.03	EXT
8	0.02	COMP
9	0.01	COMP
10	0.01	COMP

Table 22: Clustering analysis of compound Quino1 in water (distance cutoff: 3.0 Å). The Table lists the 10 most populated clusters accounting together for 78% of the equilibrium ensemble. For each cluster the relative population and a short description of the typical structural motif are reported (COMP: compact structure; EXT: extended conformation). The population of each cluster is normalized with respect to the total equilibrium ensemble (16016 structures).

Clust	Rel. Pop.	Short Desc
1	0.32	EXT
2	0.13	EXT
3	0.07	EXT
4	0.06	EXT
5	0.05	EXT
6	0.04	COMP
7	0.03	EXT
8	0.03	COMP
9	0.03	EXT
10	0.02	COMP

Table 23: Clustering analysis of compound Quino2 in water (distance cutoff: 4.0 Å). The Table lists the 10 most populated clusters accounting together for 81% of the equilibrium ensemble. For each cluster the relative population and a short description of the typical structural motif are reported (COMP: compact structure; MED: medium compactness structure; EXT: extended conformation). The population of each cluster is normalized with respect to the total equilibrium ensemble (16016 structures).

Clust	Rel. Pop.	Short Desc
1	0.29	MED
2	0.17	EXT
3	0.12	COMP
4	0.06	MED
5	0.06	COMP
6	0.03	EXT
7	0.03	COMP
8	0.02	COMP
9	0.02	COMP
10	0.01	COMP

Chirality effects in the conformational behavior of drug-6 and drug-39 epimers in water

In Figure 7 the probability distributions of the RHS-LHS distance of drug-6R and drug-6S are reported. Both distributions are bimodal and the peak corresponding to compact conformations in both cases is centered at about 5.5-6.0 Å. The peak of extended conformations however, in drug-6S is located at about 11.0 Å and is more populated than the corresponding peak of drug-6R centered at about 8.5 Å. Correspondingly drug-6S has a higher entropy content with respect to drug-6R (see Table 1 of the main paper). In other words drug-6R appears to be more compact and less disordered in water bulk solution with respect to drug-6S, which suggests a simple experiment to test our hypothesis of a correlation between compactness and inhibition potency. If the diastereoisomeric mixture of the two epimers of drug-6 could be resolved, than we predict drug-6R to be a more powerful inhibitor than drug-6S. In order to understand how the different chirality affected

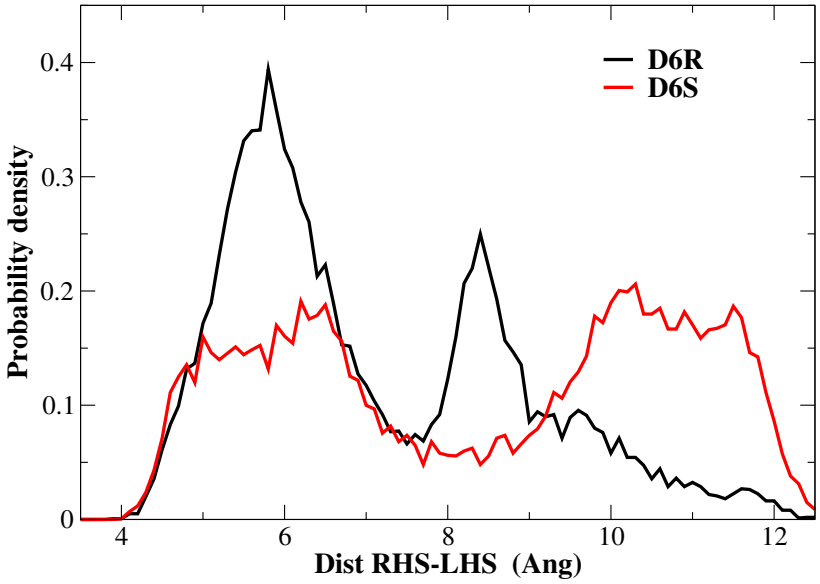

Figure 7: Probability distributions of the distance between the centers of mass of the RHS and LHS units of the two diastereoisomers of drug-6.

the probability density of the RHS-LHS distance in the two diastereoisomers, we compared the distributions of all the dihedral angles of the two species. The only relevant difference pertains

the dihedral angle of the amide bond close to the phenyl-pyrazol unit (RHS). As shown in the

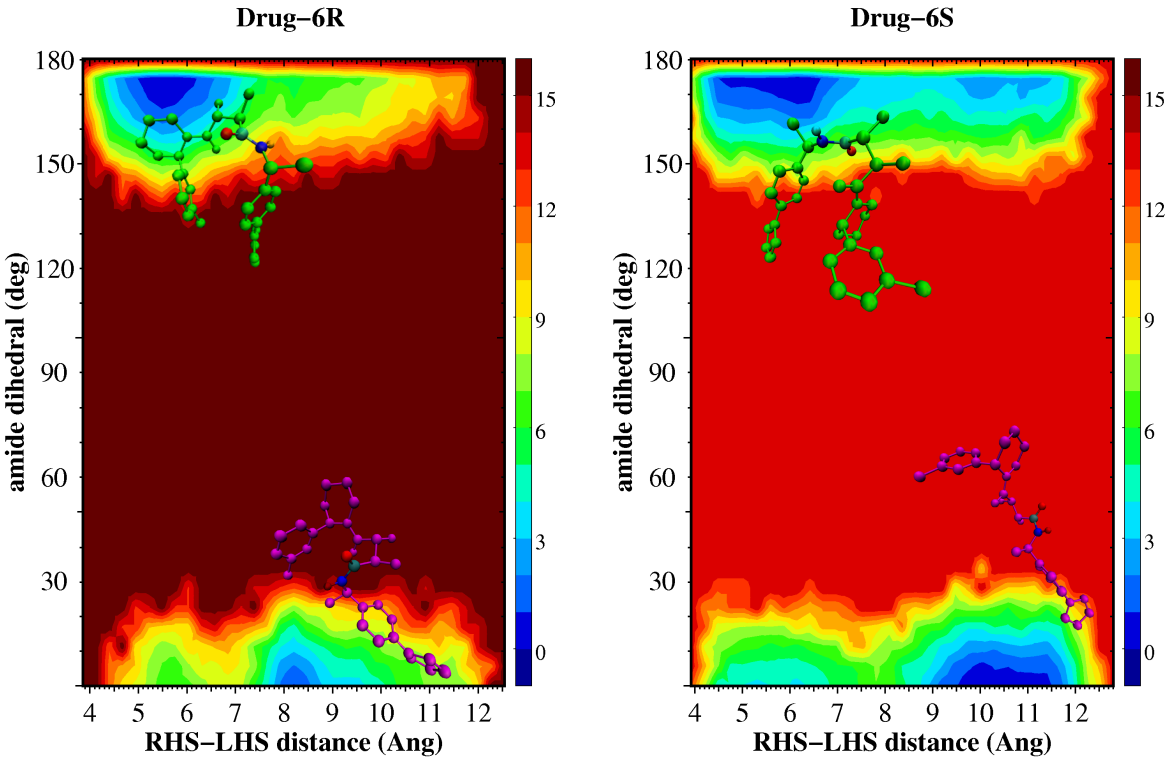

Figure 8: Free energy surface (FES) with respect to the LHS-RHS distance ($R_{\mathrm{LHS-RHS}}$, in Å) and the dihedral angel (ω in degrees) of the amide bond flanking the phenyl-pyrazol unit on the RHS in Drug-6R and Drug-6S (atoms involved in the ω torsion are highlighted). The FES is calculated using the target replica configurations as $G(\omega,\psi) = -RT \ln P(R_{\mathrm{LHS-RHS}},\omega)$, with $P(R_{\mathrm{LHS-RHS}},\omega)$ being the distribution probability of the two variables defined above. The maximum of the 2D function $P(R_{\mathrm{LHS-RHS}},\omega)$ defines the zero in the 2D FES. The energy scale (labels on the color coded bar on the right of each diagram) is in kJ mol^{-1}. Perspective views of representative structures belonging to the most populated binding clusters are reported in the 2D diagrams in the corresponding $R_{\mathrm{LHS-RHS}},\omega$ compact(*trans*)/extended(*cis*) region for both Drug-6R and Drug-6S epimers.

2D Free Energy surface with respect to the LHS-RHS distance and to the dihedral angle of the amide bond reported in Figure 8, in both diastereoisomers this amide bond can exist both in the *cis* (extended configuration) and *trans* conformation (compact state) explaining the bimodality of the distribution of the RHS-LHS distance. In drug-6S the *cis* extended conformation is characterized by a deeper and wider minimum with respect to what observed in drug-6R in agreement with the

greater abundance of extended conformations in the former isomer. The characterization of the equilibrium ensemble of drug-6R and drug-6S can be completed by a Quality Threshold clustering analysis with a cutoff of 2.0 Å. Figure 8 shows the representatives of typical clusters of compact and extended conformations of the two drugs. Both compact and extended conformations of the two diastereoisomers are quite similar, the only unavoidable difference being related to chirality. For instance, when superimposing the pyrazol-phenyl moiety in the compact structures of drug-6S and drug-6R we find that the chloro-phenyl group projects in opposite directions.

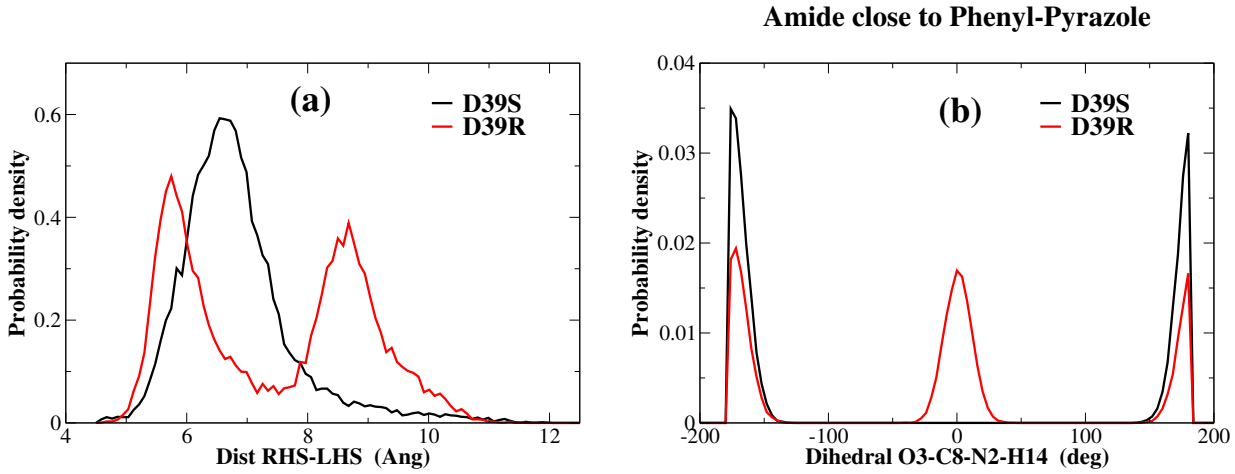

Figure 9: Equilibrium structural properties of drug-39. (a) Probability distributions of the distance between the centers of mass of the RHS and LHS units of the two diastereoisomers of drug-39. (b) Probability distribution of the dihedral angle of the amide bond close to the phenyl-pyrazol unit in the two diastereoisomers of drug-39.

Chirality has a deep effect also on the structural distribution of the isomers of drug-39. In fact, as shown in Figure 9, while the distribution of the RHS-LHS distance of drug-39R is markedly bimodal with a peak of very compact conformations centered at 5.5 Å and a peak of extended structures at 8.5 Å, the distribution of drug-39S shows a single peak of compact conformations centered at 6.5 Å and a long but flat tail vanishing at about 11.0 Å. It can thus be noted that even if some conformations of drug-39R are characterized by a shorter mean LHS-RHS distance than the compact conformations of drug-39S, the latter represent almost the totality of the equilibrium ensemble and therefore drug-39S is overall more compact than drug-39R and we predict it to be a more powerful TACE inhibitor than the cognate diastereoisomer. Similar to the case of drug-6,

the different chirality of drug-39S and drug-39R exerts its effect on the dihedral angle of the amide bond close to the phenyl-pyrazol moiety. As illustrated in Figure 9, the effect is even more marked than in drug-6. In fact, while in drug-39R this amide bond can exist both in the *cis* and in the *trans* conformation paralleling the bimodality of the distribution of the RHS-LHS distance, in drug-39S only the *trans* conformation is allowed, in agreement with the single peak in the distribution of the RHS-LHS distance of drug-39S.

Tartrate inhibitors in DMSO

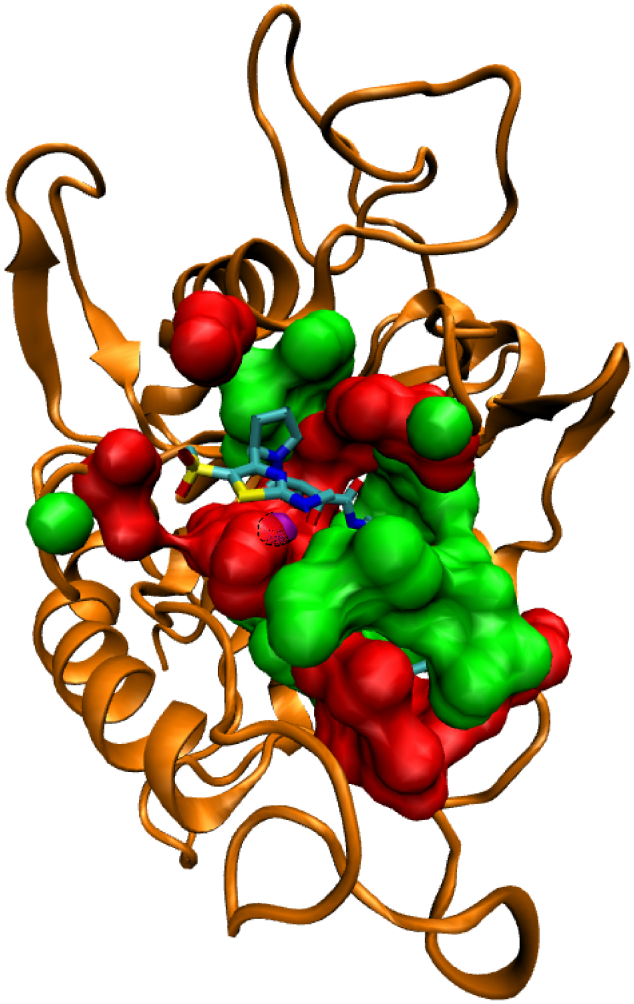

Figure 10: Hydrophobicity map of TACE active site (PDB ID: 3O64). The green and red regions represent the hydrophobic and polar residues within 6.0 Å of drug-38 respectively. The Zinc ion is represented as a purple bead.

In order to understand the structural effect of the local amphiphilic environment surrounding the tartrate drugs (see Figure 10 and discussion in subsection "Media effects on ligand conformations and TACE binding mechanism" of the main paper) once bound to the enzyme in the hypothetical intermediate, we performed Hamiltonian REMD simulations of the most powerful in-

hibitors of the series (drug-1, drug-38, drug-43 and drug-44) in dimethyl-sulfoxide (DMSO) using the same computational protocol employed for the simulations in water. The structural ensemble of the target replica was characterized through three parameters: the radius of gyration R_g, the distance between the centers of mass of the RHS and LHS groups d_{RL}, and the RMSD of heavy atoms from the average structure. As shown in Figure 12 and Figure 13 the hydrophobic environment of DMSO tends to make the distributions of the radius of gyration and of the RHS-LHS distance broader and shifted toward higher values which is suggestive of the appearance of a more extended population. In the case of drug-1 the distribution of d_{RL} in water was characterized by a main very sharp peak of compact conformations and a hump of more extended configurations. In DMSO the hump basically disappears, the only remnant being a shoulder in the single peak of the new distribution. This pattern is even more evident in the case of drug-43 and drug-44 whose d_{RL} distributions in water are bimodal. In DMSO the peak of compact conformations decreases maintaining almost unchanged its location, while the peak of extended conformations is significantly shifted toward lower values of d_{RL} (from 9.0 Å to 7.0 Å) so that the overall appearance of the new distribution is that of a single peak split in two smaller sub-peaks. Interesting information is also provided by the distributions of the RMSD from the average structure. This parameter in fact acts as an indicator of the structural uniformity of the population. As shown in Figure 11 in the case of drug-1, drug-43 and drug-44 the distribution shifts toward lower values indicating the establishment of a more homogeneous population. This is the expected result of the disappearance of the minor peak of extended conformations that was typical of the distributions in water. The removal of this eccentric conformations makes the population more closely packed around the centroid. Interestingly, drug-38 exhibits the opposite pattern with a broadening and a shift of the distribution toward higher values. As shown in Figure 9 , in water the population of drug-38 was almost exclusively composed by very compact conformations. The hydrophobic environment of DMSO loosens the hydrophobic interactions between the RHS and LHS groups that can to some extent move apart causing the reported shift of the distribution. The structural interpretation of the distributions discussed so far, can be attained through a Quality Threshold clustering of the equi-

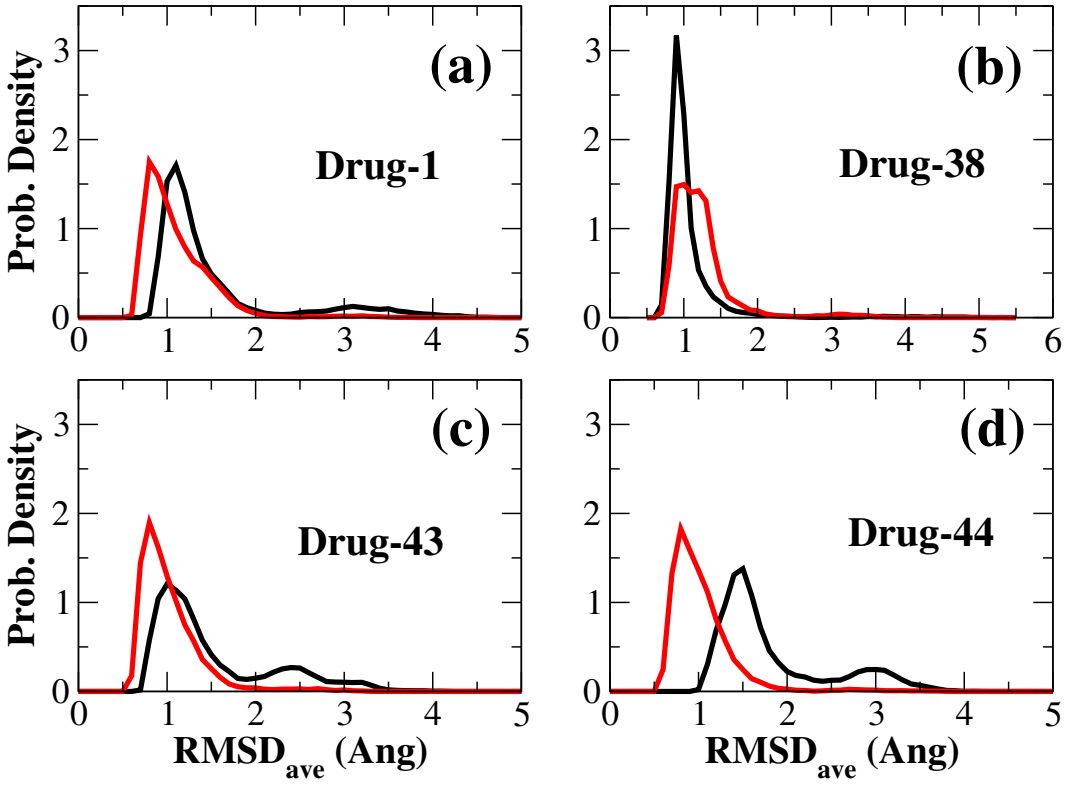

Figure 11: Distribution of the RMSD of heavy atoms from the average structure of drug-1, drug-38, drug-43 and drug-44 in water (black line) and DMSO (red line).

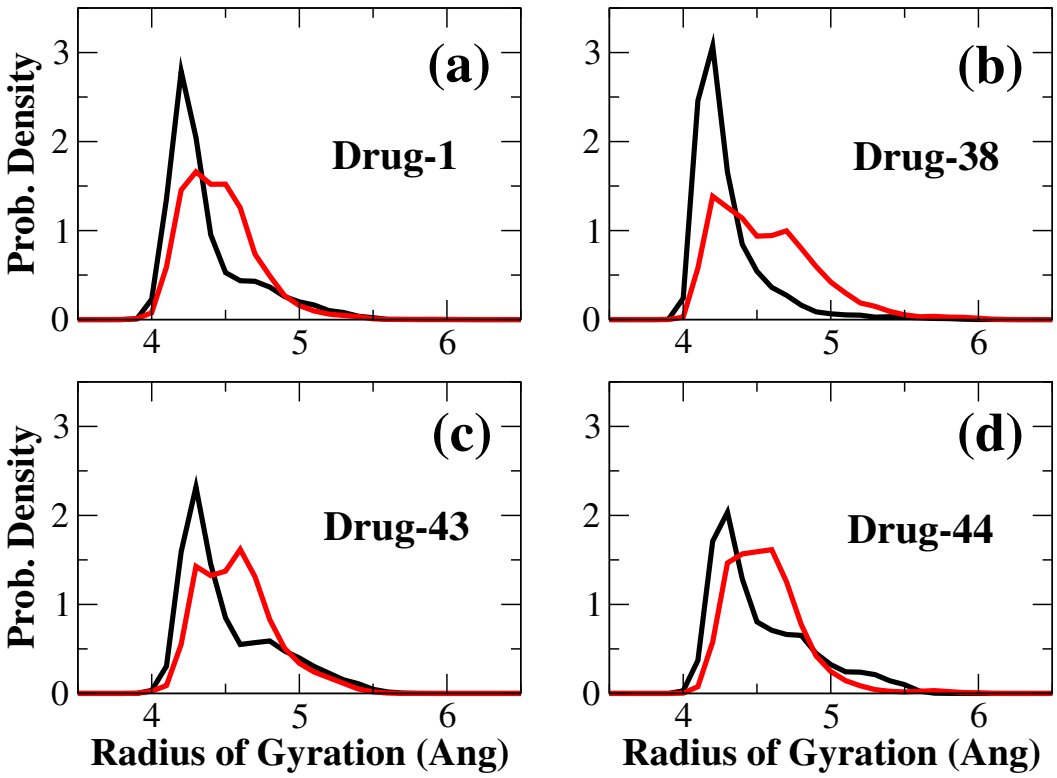

Figure 12: Distribution of the radius of gyration of drug-1, drug-38, drug-43 and drug-44 in water (black line) and DMSO (red line).

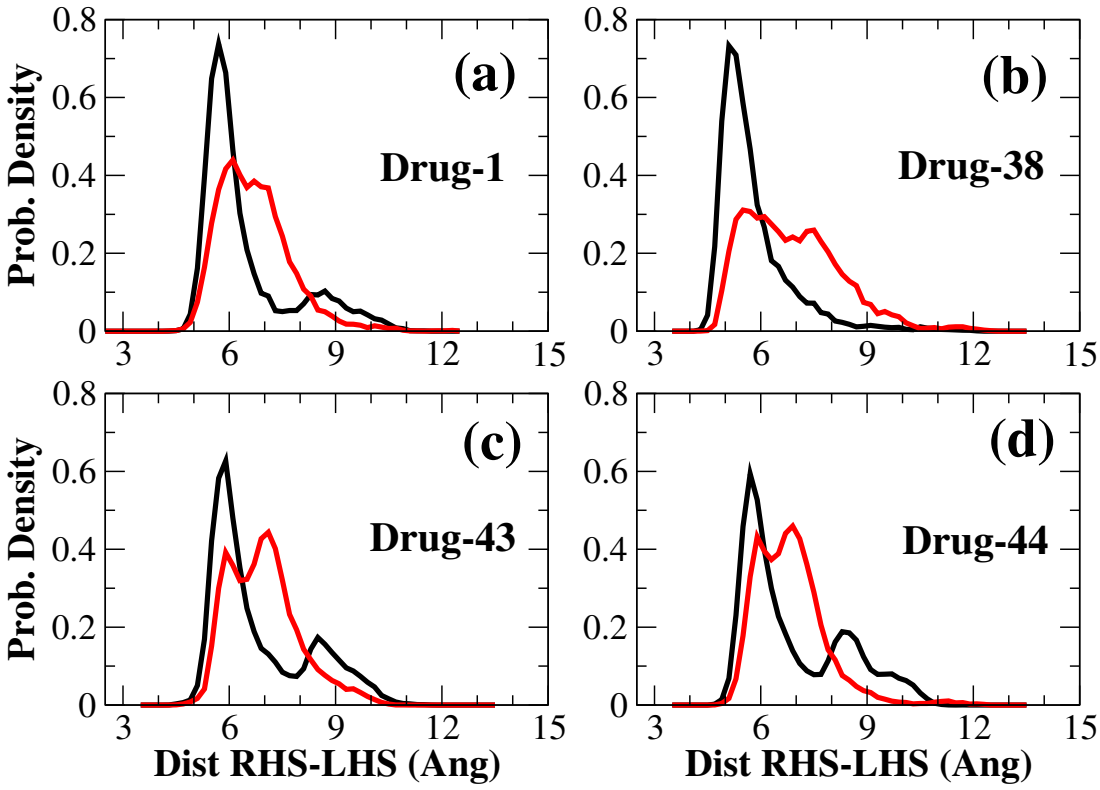

Figure 13: Distribution of the distance between the centers of mass of the RHS and LHS groups of drug-1, drug-38, drug-43 and drug-44 in water (black line) and DMSO (red line).

librium ensemble with a cutoff of 3.0 Å. In all of the four drugs simulated in DMSO it is possible to identify two main structural families of compact and extended conformations, the former family being more populated than the latter. Contrary to what occurs in the water environment, however, there is no discontinuity between the two families as reported in Figure 14 and Figure 15. For instance in drug-1 and drug-38 the 10 most populated clusters include 98% and 83% of the whole population respectively. In drug-1 four of these ten clusters corresponding to 22% of the whole

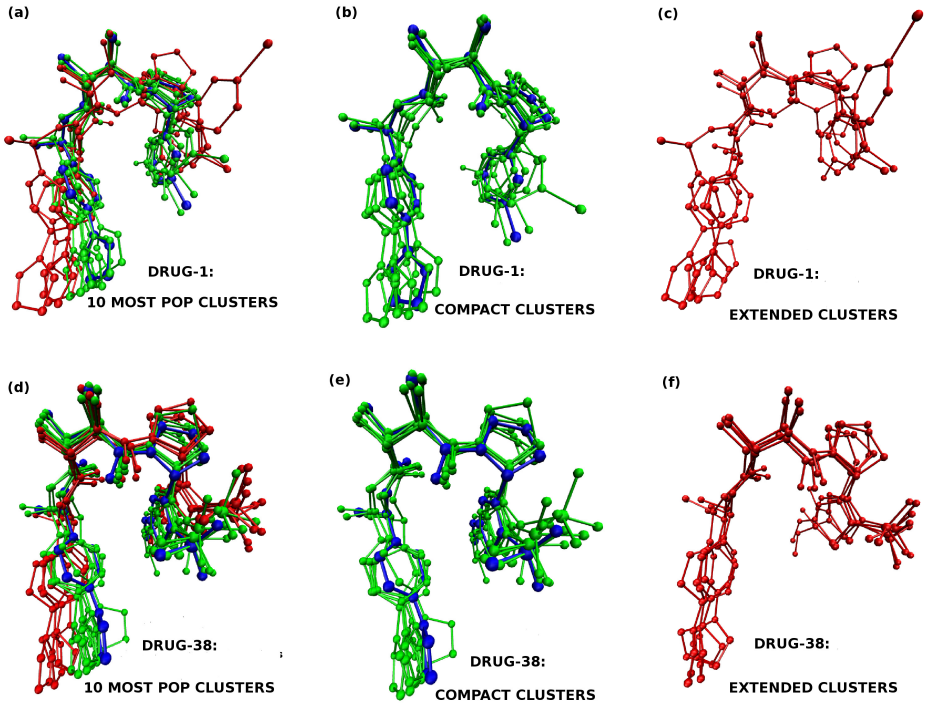

Figure 14: Structural motifs of drug-1 (first row) and drug-38 (second row) in DMSO. Panels (a) and (d) show the overlay of the representatives of the 10 most populated clusters. Compact and extended conformations are highlighted in green and red respectively and shown again independently in panels (b), (e) and panels (c), (f). The blue structure is the representative of the most populated cluster identified in water.

population comprise extended conformations while the remaining 6 clusters amounting to 76% of the population include compact structures. When the representatives of these 10 clusters are superposed using heavy atoms as shown in Figure 14, it is apparent that extended conformations are only slightly more divaricated than compact ones. There is no structural gap between the two groups and the most extended conformations of the compact family are practically undistinguishable from

the most compact structures of the extended group. The structural impact of the DMSO solvent can be better appreciated by overlaying also the representative of the most populated cluster identified in the water simulation. Figure 14 shows that the dominant water conformation is comparable to the most compact structures of the compact group equilibrated in DMSO. The situation of drug-43 and drug-44 is almost identical to that of drug-1. The 10 most populated clusters of drug-43 and drug-44 comprise 98% and 99% of the whole population respectively and the compact structures amount to 71% and 70% of the population while the extended family in both cases represents 28% of the total population. The pattern exhibited by drug-38 despite being identical to that of the other drugs from a qualitative point of view, exhibits interesting quantitative differences. In this drug the 10 most populated clusters account for 83% of the whole population the compact and extended families amounting to 51% and 31% of the full equilibrium ensemble. It thus appears that in drug-38 the destabilizing effect of DMSO is stronger than on the other drugs generating a larger group of extended conformations. This effect becomes even more pronounced if the

Table 24: Structural composition of the equilibrium population of drug-1, drug-38, drug-43 and drug-44 in DMSO. The first column indicates the consistency of the 10 most populated clusters with respect to the whole population. The second column reports the ratio of the compact conformations found in the ten most populated clusters with respect to the total equilibrium ensemble. The third column details the percentage of the extended conformations of the ten most populated clusters with respect to the full population. In parenthesis we report the relative abundance of compact and extended conformations within the ten most populated clusters.

Species	10 clust	Comp	Ext
Drug-1	98%	76% (77%)	22%(23%)
Drug-38	83%	51% (62%)	31%(38%)
Drug-43	98%	71% (71%)	28%(28%)
Drug-44	99%	70% (71%)	28%(28%)

ratios are computed with respect to the population of the 10 most populated clusters instead that respect to the whole population. In this case drug-38 features 62% compact conformations and 38% of extended ones while in the other drugs the percentage of extended conformations is always below 30%. The data are summarized in Table 24. The larger amount of extended conformations

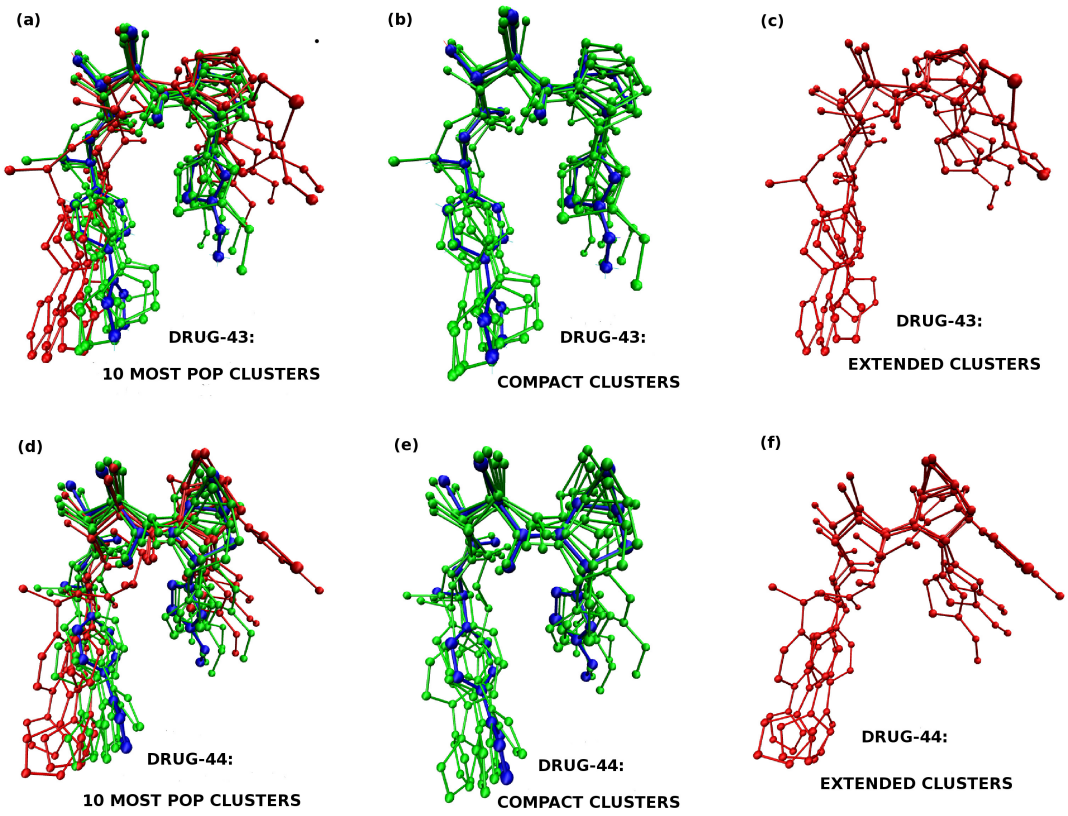

Figure 15: Structural motifs of drug-43 (first row) and drug-44 (second row) in DMSO. Panels (a) and (d) show the overlay of the representatives of the 10 most populated clusters. Compact and extended conformations are highlighted in green and red respectively and shown again independently in panels (b), (e) and panels (c), (f). The blue structure is the representative of the most populated cluster identified in water.

in the DMSO equilibrium ensemble of drug-38 highlights a twofold source of the high inhibition potency of this drug. On the one hand, the equilibrium ensemble of this molecule in bulk water is dominated by compact conformations that optimally expose the Zinc binding hydroxyl groups maximizing the probability of forming an intermediate bound complex with TACE; on the other hand the large amount of extended conformations of this molecule in DMSO suggests an efficient conformational transition to an extended configuration in the local hydrophobic environment of the active site of the enzyme. Drug-38 is thus more efficient than the other drugs in both steps of the hypothetical docking mechanism suggested by our computations.

Crystal-like conformations in DMSO

The two-state docking mechanism that we envisage foresees a structural rearrangement of the drugs once exposed to the hydrophobic micro-environment of the TACE active site. If this hypothesis is correct, then the amount of crystal-like conformations is expected to increase when the drugs are simulated in DMSO. Figure 16 shows the distribution of the RMSD of heavy atoms of Drug-38 with respect to the crystal structure (PDB ID: 3O64). When the molecule is simulated in water, the distribution shows a single sharp peak centered at 5.0 Å suggesting only a very modest amount of crystal-like conformations. The presence of crystal-like conformations, however, may escape the RMSD analysis due to the high mobility of the methyl-sulphonil and methyl-amino groups that can freely rotate around the bonds that link them to the thiazole ring. Indeed, when the RMSD is re-computed after deletion of the two groups, the distribution slightly shifts toward lower values. Using the same approach, the RMSD was also computed after removal of the whole thiazole ring. The result is a significant down-shift of the RMSD distribution now exhibiting a single peak located at 3.0 Å and a long tail stretching down to 2.0 Å. It is interesting to compare this pattern with the results of the same analysis performed on the trajectory in DMSO. The RMSD distributions of Drug-38 with or without the methyl-sulphonil and amino-methyl groups still show a single peak at about 5.0 Å, but these peaks are lower and much broader than the corresponding peaks recorded in water and they feature a long tail extending to 6.5 Å. Thus, at first sight, the conformation of Drug-38 in DMSO is even less crystal-like than in water. This result, however, is simply the consequence of the higher entropy of the thiazole ring that in DMSO is not constrained by the hydrophobic interactions with the phenyl-pyrazole unit (stabilizing the compact conformations observed in water). As a consequence the thiazole ring can freely rotate around the bond with the pyrrolidine ring generating a large ensemble of conformations very different from the crystallographic one. When the thiazole ring is removed, however, the distribution of the RMSD moves to about 2.5 Å and is thus shifted to lower values with respect to the corresponding distribution in water. In other words, the fragment of the drug between the pyrrolidine and the pyrazole rings is very similar to the crystallographic one while the difference from the crystal can be attributed to

the rotation of the thiazole ring. This event however, does not impair the ability of the drug to fit into the S1'-S3' TACE cavity since the thiazole ring was designed to interact with the shallow and solvent-exposed non-primed pockets where some rotational freedom is allowed.

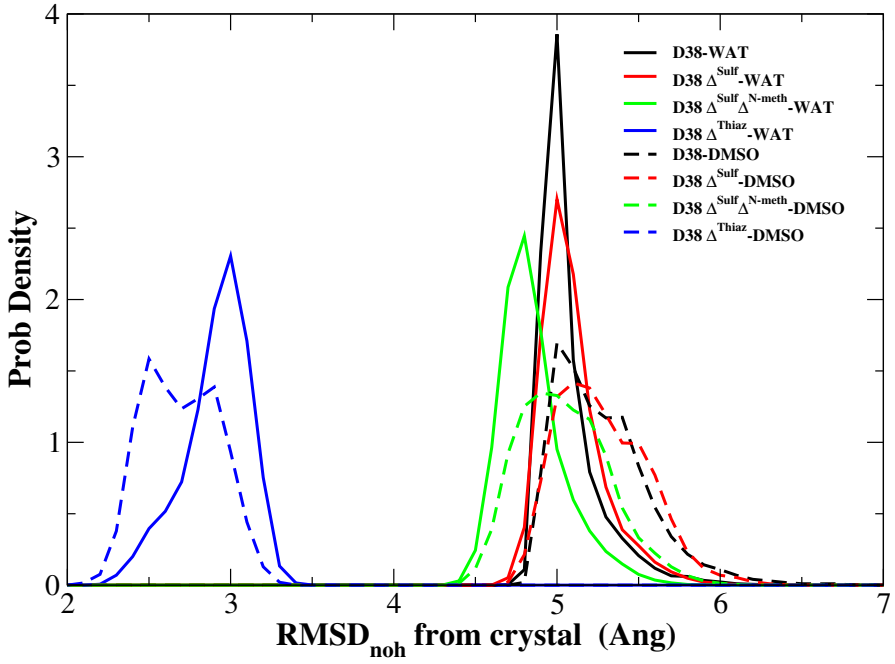

Figure 16: Probability distributions of the RMSD of heavy atoms of Drug-38 in water (solid lines) and in DMSO (dashed lines) with repsect to the crystal (PDB ID: 3O64).

A significant amount of crystal-like conformations can also be detected in the equilibrium ensemble of Drug-1, Drug-43 and Drug-44. Also in this case the alignment between the three drugs and the crystal structure of Drug-38 was performed using the heavy atoms of the common scaffold *i.e.* the regios stretching from the pyrrolidine ring to the pyrazole ring. Figure 17 shows that in all of the drugs the RMSD distribution feature a single peak approximately extending from 2.0 Å to 3.5 Å. When the calculation is repeated in the trajectory recorded in DMSO the distribution shifts to lower values which is indicative of an increase in the amount of the crystal-like conformations (that we expect to be the best suited to fit into the S1'-S3' pocket of the active site). These results are perfectly consistent with the clustering analysis (cutoff distance: 3.0 Å). In Figure 18 we show the overlays of the crystal structure of Drug-38 and the representatives of typical clusters of extended conformations of Drug-38, Drug-1, Drug-43 and Drug-44. It can be noted that the tartrate

core and the phenyl-pyrazole unit (expected to interact with the Zinc ion and the S1'-S3' pocket respectively) show an excellent overlap with the crystal structure. Conversely, the superposition of the Left Hand Side unit is less satisfactory, but this detail is rather un-relevant for the stability of the enzyme-substrate complex since the LHS group was designed to be weakly engaged with the non-primed pockets.

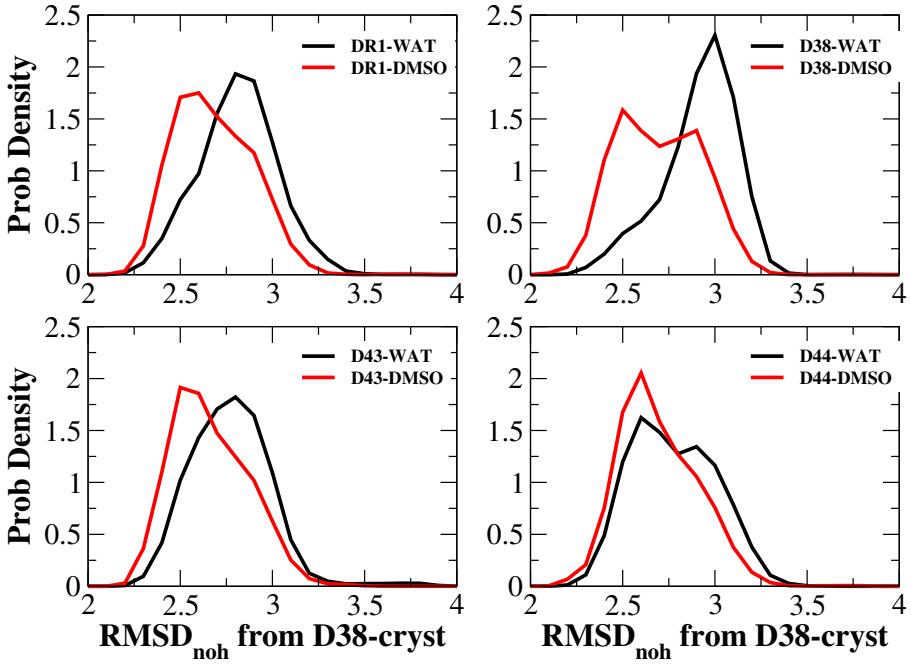

Figure 17: Probability distributions of the RMSD from the crystal structure of Drug-38 of the heavy atoms of Drug-1, Drug-38, Drug-43 and Drug-44 in water (black lines) and in DMSO (red lines).

Figure 16 and Figure 17 clearly show that when the tartrate-derived TACE inhibitors are displaced from an hydrophilic to an hydrophobic environment there is a significant increase in the amount of crystal-like, extended conformations. Within the famework of the postulated two-state mechanism the extent of this increase should correlate with the potency of the inhibitor. This issue is addressed in Figure 19 where crystal-like and non crystal-like conformations are discriminated using a cutoff value of 3.0 Å for the RMSD of heavy atoms with respect to the crystal structure of Drug-38. In Figure 19 we can then plot the logarithm of the inhibition constant as a function of the increase in the fraction of crystal-like conformations resulting from the $WAT \rightarrow DMSO$ solvent

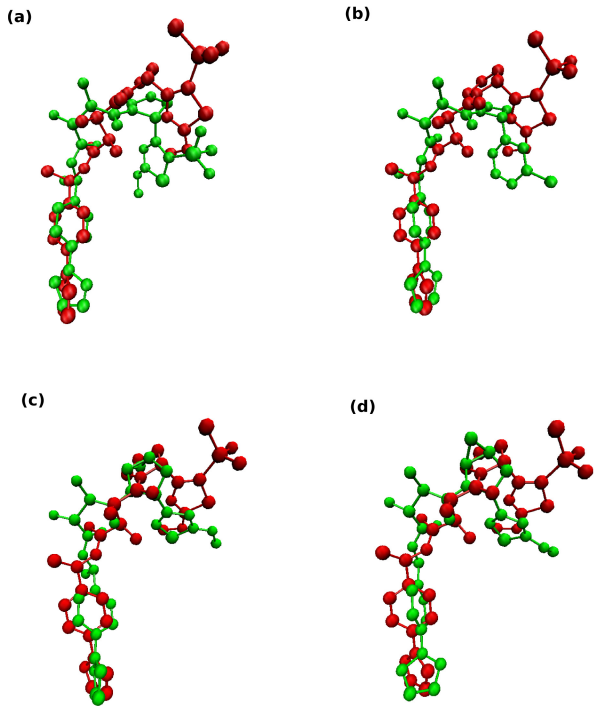

Figure 18: Overlays of the crystal structure of Drug-38 (PDB ID: 3O64; red) and the representatives of typical clusters of extended structures (green) of Drug-1 (a), Drug-38 (b), Drug-43 (c) and Drug-44 (d). The superposition has been realized so as to minimize the RMSD of the heavy atoms of the common fragment extending from the pyrrolidine ring to the pyrazole ring.

change. The correlation coefficient computed using all four points $r = -0.33$ is low because the point corresponding to Drug-44 acts as an outlier. If this point is excluded, however, the correlation coefficient increases to $r = -0.99$.

We are aware that a correlation coefficient $r = -0.99$ only using three points is not a strong evidence. While work is underway in our lab to simulate other tartrate-derived inhibitors in DMSO, we further support our conclusions studying the correlation between the logarithm of the inhibition constant and the increase in the fraction of extended conformations resulting from the $WAT \rightarrow DMSO$ solvent change. Based on the plots in Fig 2 of the main paper and Figure 13 extended and non extended conformations are discriminated based on a cutoff of 6.0 Å in the distance between the centers of mass of the RHS and LHS units. The regression line is reported in Figure 20. As in Figure 19 if the outlier (point D44) is excluded, the linear correlation is excellent ($r = -0.998$).

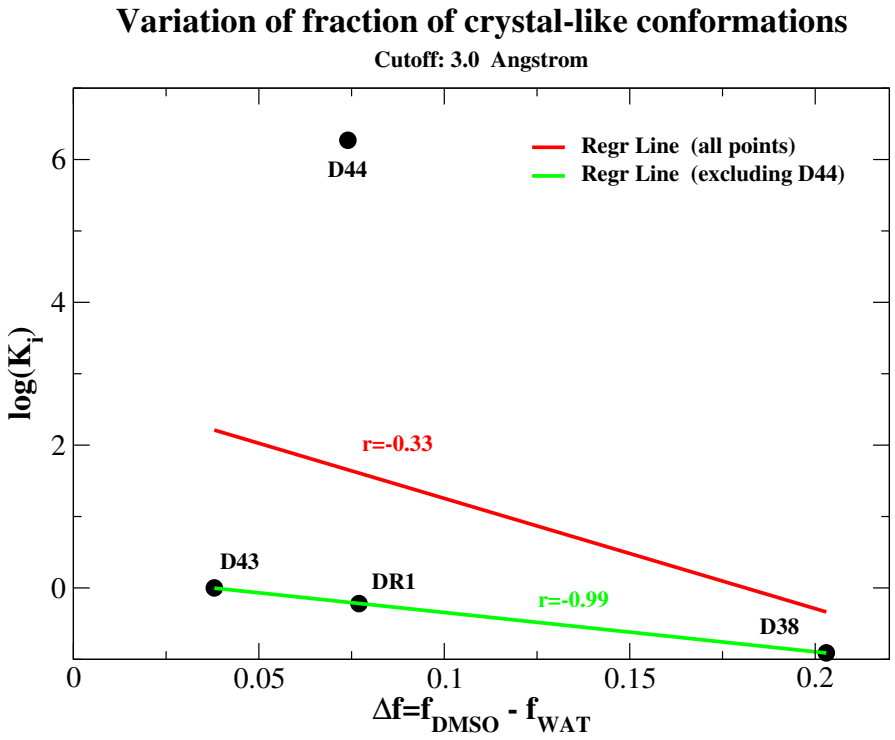

Figure 19: Regression line between the increase in the fraction of crystal-like conformations in the *WAT* $\rightarrow$ *DMSO* solvent change and the logarithm of the inhibition constant. The red line is the regression line computed using the points corresponding to Drug-1, Drug-38, Drug-43 and Drug-44. The green line is the regression line computed excluding Drug-44 that acts as an outlier.

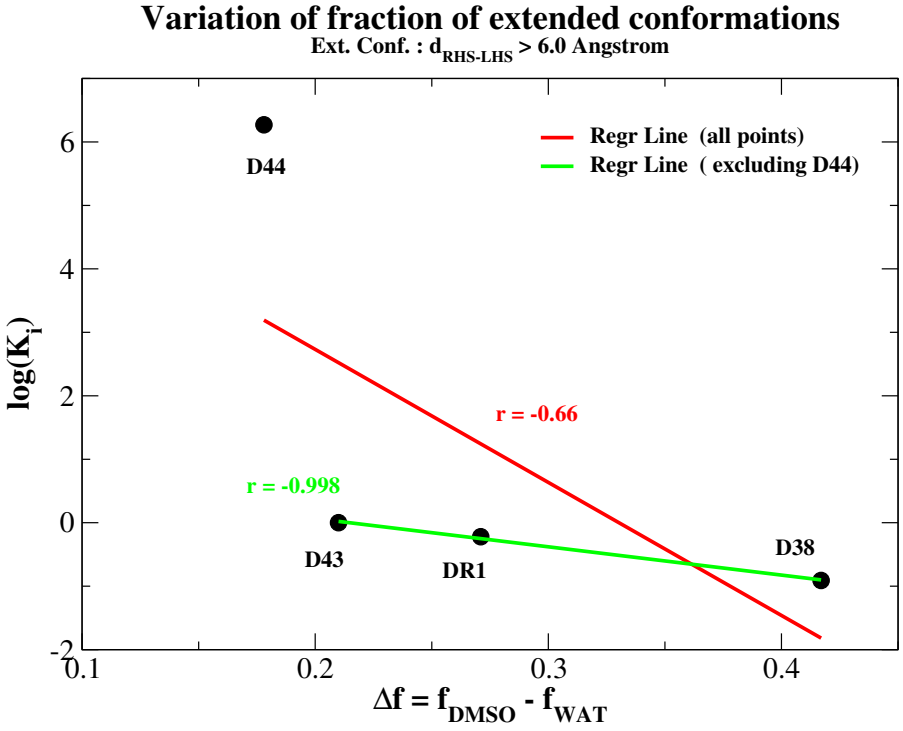

Figure 20: Regression line between the increase in the fraction of extended conformations in the *WAT* $\rightarrow$ *DMSO* solvent change and the logarithm of the inhibition constant. The red line is the regression line computed using the points corresponding to Drug-1, Drug-38, Drug-43 and Drug-44. The green line is the regression line computed excluding Drug-44 that acts as an outlier.

Docking mechanism of tartrate-based TACE inhibitor

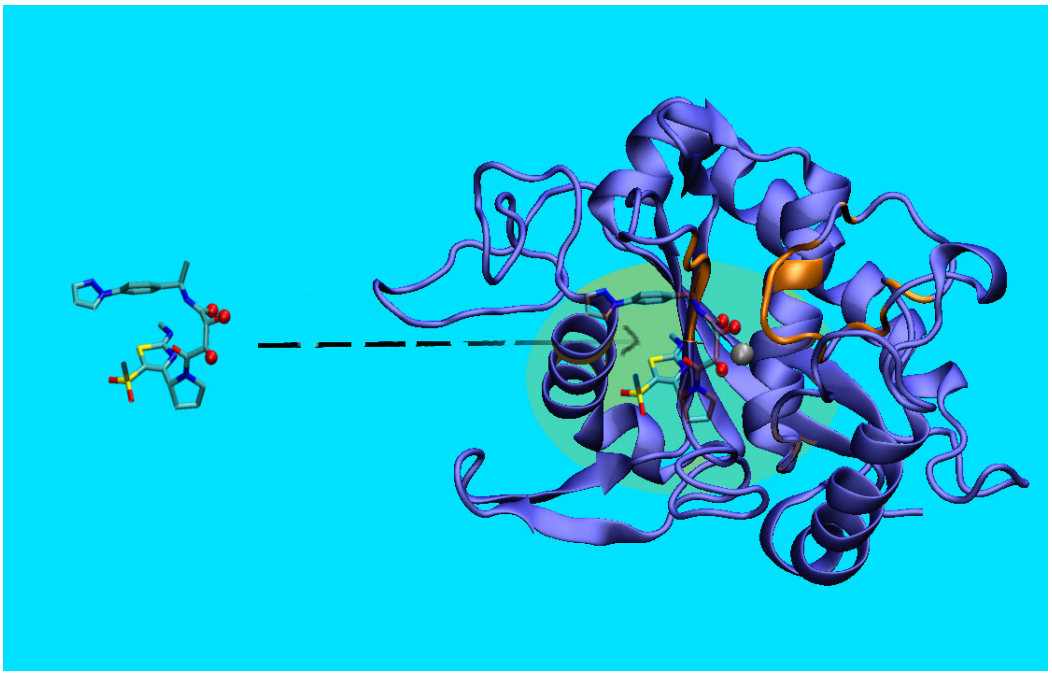

Figure 21: Step 1: the drug in its compact/low entropy conformation in water environment (cyan color) binds the catalytic zinc (gray bead) with the solvent exposed ZBG (hydroxy groups and LHS carbonyl unit)

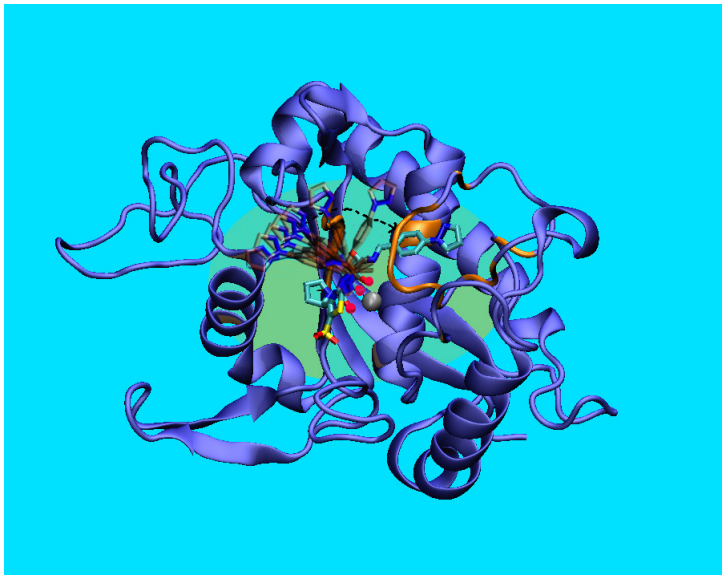

Figure 22: Step 2: when docked to the TACE, the less polar environment (green) promotes the drug reorganization and the access of the phenyl-pyrazol moiety to the primed pocket (residues in orange)